INJURY BIOMECHANICS RESEARCH
Proceedings of the Thirty-Ninth International Workshop

Blunt Injury Response of Occupant Lower Extremity during Automotive Crashes: A Finite Element Study

N. Yue[1], J. Shin[1] and C. D. Untaroiu[2]

[1] Department of Mechanical and Aerospace Engineering, University of Virginia, USA
[2] Virginia Tech and Wake-Forest School of Biomedical Engineering and Sciences, Virginia Tech, USA

ABSTRACT

More than half of occupant lower extremity (LEX) injuries during automotive frontal crashes are in the knee-thigh-hip (KTH) complex. The objective of this study is to develop a better understanding of the KTH injury mechanisms and injury thresholds using a new finite element (FE) human model. A detailed biofidelic occupant LEX FE model is developed based on the component surfaces reconstructed from the medical image data of a 50th percentile male volunteer in a sitting posture. The hexahedral element type is used to mesh the majority of the deformable skeleton and soft tissues. Appropriate constitutive material models are assigned to each component with the corresponding parameters rigorously identified in the ranges of published test data. Eight loading cases are simulated and the model's predictions are validated at both regional and global levels to the latest corresponding test data recorded in cadaveric testing. These validations are focused on the predictions of frontal Crash-Induced Injuries (CII) recorded in vehicle crashes, which includes the femoral mid-shaft/head fractures, tibia distal-third fracture, and knee ligament failures (e.g. posterior cruciate ligament (PCL)). Then, a sensitivity study is performed using the validated KTH model to investigate the effect of the hip joint angle to the acetabulum injury tolerance in frontal impacts. The results indicate a tendency of less stress concentration in the illac wing and a 16% to 36% hip injury tolerance increase with the hip joint flexion angle increasing from -30^0 to +20^0 relative to the neutral posture.

INTRODUCTION

Occupant lower extremity (LEX) injuries in automotive crashes account for 26% of AIS 2+ injuries for belted passengers (Morgan et al. 1990). 55% of these injuries occur in the knee-thigh-hip (KTH) complex and they account for 42% of the life-years lost to injury for occupants in airbag equipped vehicles (Kuppa et al. 2001). To develop a better understanding of Crash-Induced Injuries (CII) required in designing injury countermeasures, several experimental and numerical approaches have been used (Crandall et al. 2011). Experimental approaches have been tried to evaluate CII recorded in lab conditions using Post Mortem Human Subjects (PMHS) impact tests. However, inherent variations in terms of PMHS

anthropometry and material properties make it challenging to understand the injury mechanisms and to develop accurate injury criterion using test data. Recently, with rapid increase in computational power, several human numerical models have been used for vehicle safety research and development (Spethmann et al. 2009). The human finite element (FE) models are currently the most sophisticated human numerical models which can provide general kinematics of the whole human body, calculate the detailed stress/strain distributions inside the model, and can be then correlated with the risk of injuries.

Several FE LEX models were developed to investigate traffic accidents involving vehicle occupants and pedestrians. The pedestrian LEX models were designed in a standard mid-stance posture and employed in lateral vehicle-pedestrian impact simulations (Maeno et al. 2001, Takahashi et al. 2003, Untaroiu et al. 2005). In addition, several occupant LEX FE models were developed in a standard sitting posture. Schauer et al. (1997) developed an occupant KTH FE model which was later improved by Silvestri et al. (2009) to study the injury mechanism of KTH during frontal impact. The geometry of the bones was reconstructed from the Visible Human (VH) dataset. The soft tissues, such as muscles, tendons and ligaments, were modeled using one-dimensional discrete elements, whose attachment points to the bone models were approximated based on literature data. The model was validated against component tests (e.g. the femur impact, femur-pelvis impact, femoral condyles impact) and whole-body frontal impact tests. Kim et al. (2005) also developed an occupant KTH FE model based on the geometries reconstructed from the VH dataset (pelvis, acetabulum, and proximal femur) and the medical scans of a 50^{th} percentile male volunteer (LEX). The model was validated against the data recorded in component tests (three-point bending test of the femur, axial loading of the isolated knee with patella, axial loading of the isolated knee with a padded impactor, stance-like loading of the femoral head, axial loading of the KTH complex) and a frontal whole body PMHS sled test. Other LEX FE models include the H-Model developed by Haug et al. (2001) and the LEX model developed by Beillas et al. (2001).

The main limitations of existing lower limb FE models come from their geometries, the modeling approaches used to represent their components, and limited test data used for model validation. In some models, the whole lower limb geometry or some of their components were obtained by uniformly scaling the geometry of the VH dataset (Silvestri et al. 2009, Kim et al. 2005). This approach inherently introduced some local inaccuracies of the model. In other models (e.g. Hung et al. 2001, Beillas et al. 2001, Silvestri et al. 2009), the geometry of ligaments and thicker layers of cortical bone were simplified by modeling those components as bar and shell elements, respectively. Finally, all previous models could not benefit from the huge amount of material and component test data published recently.

The objective of this study is to develop a more biofidelic occupant LEX FE model using the geometry directly reconstructed from the computed tomography (CT)/magnetic resonance imaging (MRI) scan data of a 50th percentile male volunteer. The model includes accurate representations of the cortical and trabecular layers of the femur, tibia, fibula and patella, knee cartilages, knee and hip joint ligaments, menisci, knee tendons, beam thigh muscle, hip joint capsule, flesh, and skin. The material properties were rigorously defined based on the appropriate literature data and the model was comprehensively validated against the latest test data of femoral shaft three-point bending test (Funk et al. 2004), femoral shaft combined axial compression and bending loading test (Ivarsson et al. 2009), femoral head quasi-static compression tests in both stance and fall configurations (Keyak et al. 1998), leg combined axial compression and bending loading test (Untaroiu et al. 2008), knee ligament (PCL) shear loading test (Balasubramanian et al. 2004), knee-thigh (KT), and KTH impact tests (Rupp et al. 2003). Finally, the injury tolerance of KTH for various hip joint angles was evaluated to better understand the mechanism of acetabulum fractures observed in frontal crashes.

METHODS

1. Development of the thigh-knee-leg FE model.

The geometry reconstruction process of the occupant LEX was conducted by the Center for Injury Biomechanics, Virginia Tech-Wake Forest University (Gayzik et al. 2011). A male volunteer with anthropometric characteristics (175.3 cm height and 77.1 kg weight) close to the 50th percentile male (175.3 cm/78.2 kg- Hybrid III dummy, 175.8 cm/78 kg- Gordon et al. 1988) was recruited to develop an extensive image data set. The resolution/ thickness of the CT and MRI scans were 0.98/ 1.25 mm and 1.5/ 1.6 mm, respectively. The geometries of the bony structures and soft tissues of the volunteer LEX region were reconstructed using the CT and MRI scanned images, respectively. The knee flexion angle of the scanned LEX was about 120^0 to mimic the seating posture of the occupant LEX in a vehicle (Robbins et al. 1983).

Meshing

Two meshing approaches, structural and unstructural, were employed to achieve a good quality hexahedral mesh. The structural mesh technique consists of filling the solid object with cubic blocks (the mesh topology) and projecting the outer and inner boundaries to the exterior and interior surfaces of the object. Structural IA-FEMesh (University of Iowa, Iowa City, IA), TrueGrid (XYZ Scientific Applications, Livermore, CA) and HyperMesh 10 (Altair HyperWorks, Troy, MI) were used to mesh the tibia, fibula, knee ligaments (anterior cruciate ligament (ACL), posterior cruciate ligament (PCL), medial collateral ligament (MCL) and lateral collateral ligament (LCL)), knee tendons (femoral and tibial), menisci (medial and lateral), and flesh. The cortical bones in the diaphysis regions of the tibia and fibula were meshed by HyperMesh 10 and the trabecular bones in the epiphysis regions of those long bones were meshed by IA-FEMesh. Then the diaphysis was connected to the corresponding epiphysis regions of those long bones to smooth the transitions from the solid to the shell cortical layers (Fig. 1). The unstructural technique (grid-based hex meshing) creates approximately same-sized hex elements in the interior of the model. Then, the marginal hex elements are projected on the model boundaries. This approach is efficient for meshing models with complex geometries by using the fine and high quality hex elements inside the models. Even though some poor quality elements may be inherently generated at the boundary of the volume, mesh optimization algorithms are usually used to improve their qualities. The unstructural HexMesher in Morpher 5.0 (Detroit Engineering Products, Troy, MI) was employed to mesh the femur and patella which require finer mesh with high quality elements for better fracture predictions in frontal crashes. The element size of the bony structures and most of the soft tissues (except flesh) generally ranges from 1.5 mm to 3 mm, taking into consideration of both the computational accuracy and efficiency. The larger element size (~ 8 mm) was used for the flesh which is mostly responsible for impact energy absorption and transmission. While flesh injury is not life-threatening, the prediction of these injuries was out of the scope of this study. Shell elements were employed to mesh the thin layers of cortical bone in the epiphysis regions (thickness of 1.0 to 4.0 mm, Brown et al. 1984) in order to keep the simulation time steps at reasonable values considering current computational power (0.35% mass added by mass scaling for 0.3 μs time step). The cortical shell elements shared the nodes with the inner trabecular solid elements and their nodal thicknesses were individually calculated by a customized MATLAB code (MathWorks, Natick, MA). The cartilages (femoral, patellar, medial and lateral tibia plateau) were represented by quadrilateral shell elements with nodal thicknesses assigned by the same MATLAB code.

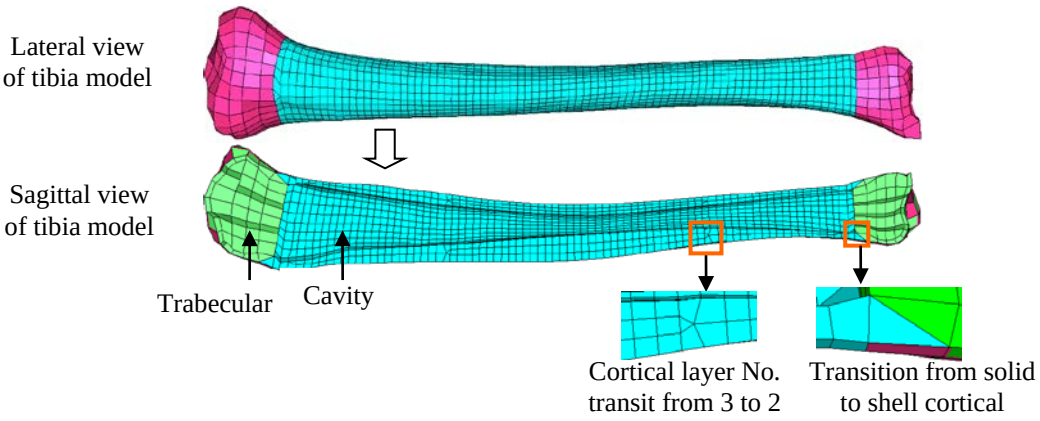

Figure 1 The mesh of FE tibia and the smooth transitions from solid to shell cortical bone layer (Untaroiu et al. 2012).

First, the normal $\vec{n}$ of a shell element on the outer surface of the cortical bone was calculated at a designated node. Then, a cluster of nodes inside of a sphere with the center at the designed node and a chosen search radius (e.g. 5 mm) were identified. For each node in the cluster, the position vector $\vec{r}_i$ and the angle between this vector and the normal θ_i were calculated. The projection of each position vector along the normal was calculated and the minimum projection was defined as the shell thickness (Fig. 2). While a node may belong to several surrounding shell elements with different normals, all calculated thicknesses of a node were averaged to find a unique thickness for a node which was written automatically in a LS-Dyna (LSTC,

Livermore, CA) format. The shell elements of cortical bone shared the nodes with the shell elements of the cartilage layer, but their reference surfaces were defined with an offset (above –cartilage and under-cortical bone) from the plane of the nodal points to avoid overlapping. (LS-DYNA, manual).

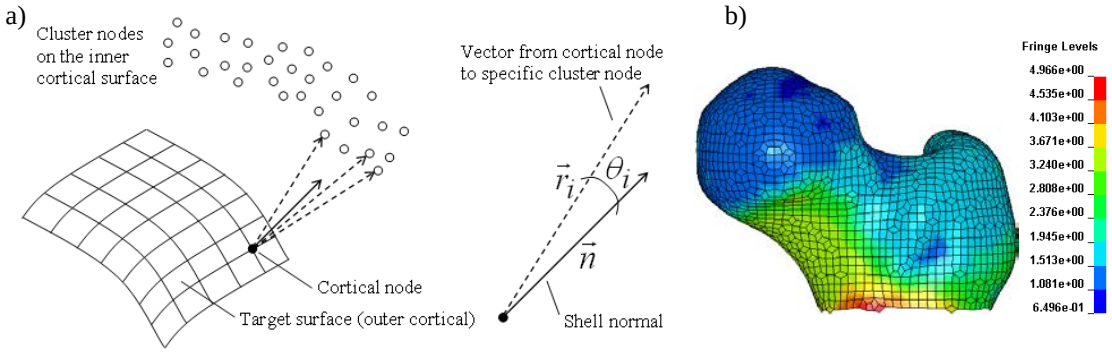

Figure 2 a) Schematics of MATLAB code thickness calculation algorithm, b) femoral head cortical shell thickness distribution (Untaroiu et al. 2012)

Material models and properties

Material models included in the library of the explicit and implicit LS-DYNA 971.R4 FE solver were assigned to all lower limb parts. The cortical and trabecular bone were modeled as an elastic-plastic material. The bone material models were assumed to be isotropic and have similar mechanical properties in tension and compression loading, due to the lack of more complex material models for bone in the LS-DYNA material library. Cortical bone fracture was modeled by the element elimination method, with the fracture threshold of 0.88% effective plastic strain (Untaroiu et al. 2004). Literature data shows that the femoral head subchondral bone in the weight-bearing region has an elastic modulus of approximately 1.5 GPa (Brown et al. 1984), which is much lower than the corresponding value in the shaft region (6-21 GPa, Keller et al. 1990, Currey et al. 1997 and Untaroiu et al. 2010). In addition, the elastic modulus of the cortical shell in the femoral neck region is 24% less than the shaft region (Lotz et al. 1991). Based on these literature data, the cortical bone layer of the proximal femur was divided into three small sub-components: the femoral head, the femoral neck and the connective femoral shaft with elastic modulus of 2 GPa, 6 GPa and 13.5 GPa, respectively (Fig. 3a). On the other hand, literature data suggest that the stiffness and strength of femoral head trabecular bone have a decreased trend from femoral head to shaft region (Fig. 3b). Thus, the elastic modulus of femoral head trabecular bone was individually assigned to the subchondral region, the femoral neck, and the intertrochanter with values of 0.7 GPa, 0.4 GPa, and 0.2 GPa (Martens et al. 1983, Evans and King 1961). The yield stress of each respective component in the proximal femur region was scaled proportionally to its corresponding elastic modulus. A quasi-linear viscoelastic (QLV) material model (MAT_92, LS-DYNA manual) was assigned to the knee ligaments to provide transversely isotropic material symmetry with high stiffness along the fibers (parallel to the normal of the assigned hexahedral element) in tension and negligible stiffness in compression or along directions included in the transverse plane. Knee ligament rupture threshold was defined as the maximum principal strain of 0.4 (Takahashi et al. 2000). The flesh was defined as a simplified rubber/foam model with the dynamic engineering compressive stress-strain curve defined by Untaroiu et al. 2005 and tensile stress-strain curve defined by Yamada 1970. The elastic modulus of the hip joint ligaments was assigned as 0.15 GPa which is in the range value reported by Hewitt et al. 2001 (0.076 - 0.286 GPa). The rest of the soft tissue material models and their initial parameters were assigned accordingly (Table 1) based on a previous pedestrian LEX FE model (Untaroiu et al. 2005).

While a full integration scheme was used for shell elements, a one point integration scheme with constant stress was used for solid elements. The LS-DYNA hourglass types of standard viscous form and Flanagan-Belytschko stiffness form with exact volume integration were used for soft tissues and bony structures, respectively. After the left lower limb FE model was developed, the corresponding right lower limb was created by reflection along the middle sagittal plane of the specimen.

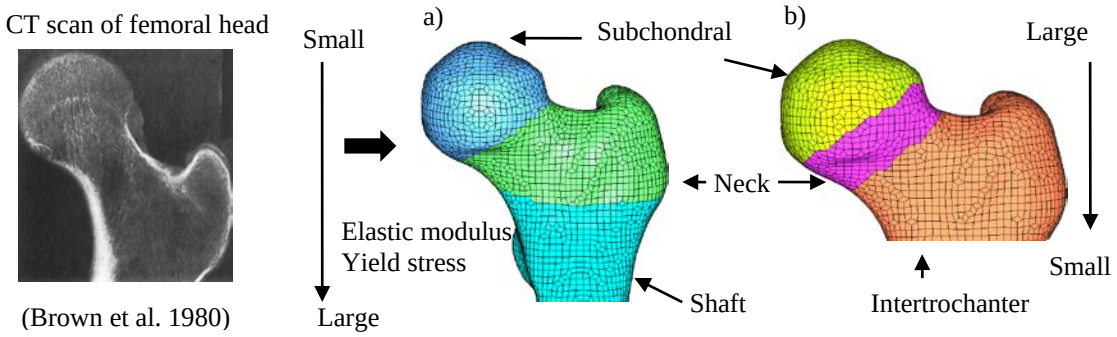

Figure 3 Proximal femur material properties of a) cortical bone and b) trabecular bone (Untaroiu 2012).

2. Validation of the thigh-knee-leg FE model

Femoral shaft three-point bending

While the biomechanical response of femur plays an important role in the global mechanical response of the occupant LEX during vehicle crashes, the femoral regions were validated to the main loading observed in frontal and side impacts. Initially, the femoral shaft was validated against the data recorded in dynamic three-point bending loading tests (Funk et al. 2004). As in testing, the femoral epiphyses were mounted into the rolling cups to approximate the rotation centers of the femoral joints. A cylindrical rigid impactor with a diameter of 12 mm was positioned at the mid-shaft location of the femur and then was used to impact the specimen along the posterior-anterior (P-A) direction (Fig. 4a). The velocity time history (with about 1.2 m/s initial velocity) recorded in testing was imposed to the impactor model and the impactor contact force was calculated during the FE simulation. While some of the PMHS used in the tests by Funk et al. (2004) had larger body sizes, the force-displacement data was scaled based on the dimension of current model which was assumed to represent a 50th percentile male. The length scale factor λ_L and the mass scale factor λ_m were calculated as the ratio of the specimen data to the data of the standard 50th percentile male (Untaroiu et al. 2005). The equivalent scale factor was defined as $\lambda_{eq} = (\lambda_m \lambda_L)^{0.25}$ (Irwin et al. 2002) and the time and force scale factors were defined as $\lambda_t = \lambda_{eq}$ and $\lambda_F = \lambda_{eq}^{\ 2}$, respectively. The ranges of the calculated scale factors of time and force for femur specimens were 1.022 ± 0.056 and 1.046 ± 0.113, respectively. The force-displacement recorded in the simulation was compared with the corresponding test data scaled using the procedure mentioned above.

Femoral shaft combined loading

The femoral shaft model was further validated against dynamic combined (bending and compression) loading based on test data reported by Ivarsson et al. 2009. In testing, the femoral epiphyses were mounted into the potting cups, which can translate along the femoral shaft longitudinal direction and rotate into the sagittal plane. All degrees of freedom in other directions were constrained (Fig. 4b). First a compression preload was applied along the axial direction of the femoral shaft using a ramp law up to 20 ms. Then, an aluminum half-cylinder impactor (diameter of 25.4 mm), with a displacement rate of 1.5 ms, impacted a small piece of foam padding of thickness 6.2 mm positioned on top of the specimen and ramps it to failure in three-point bending. The material model of the foam represents highly compressible low density foam (MAT 57, LS-DYNA manual) with the stress-strain curve defined by dynamic (20 mm/s) compression data reported by Ivarsson et al. 2009. The model was impacted along both posterior-anterior (P-A) and anterior-posterior (A-P) directions, with compression preloads of 0, 4, 8, 12, and 16 kN. The bending moment induced by the impact force at the time of bone fracture was calculated for each case based on Eq. 1 and used for validation.

$$M_{fracture} = F_{fracture} L / 4 \quad (1)$$

Where $F_{fracture}$ is the impact force at bone fracture and L is the femur shaft length.

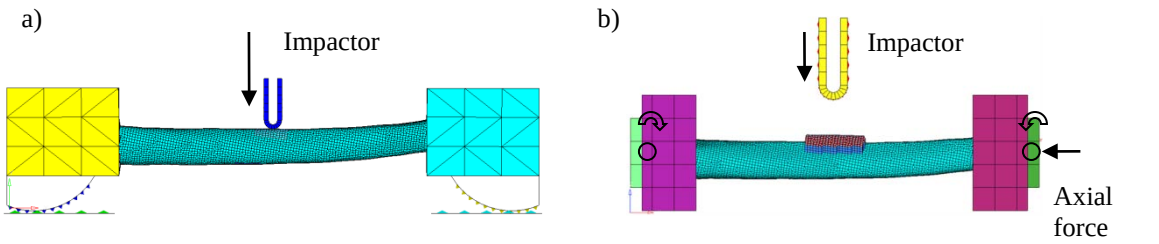

Figure 4. Femoral shaft a) three-point bending and b) combined (P-A) loading FE model setup (Untaroiu et al. 2012).

Table 1 Material models and corresponding parameters.

ID	Material Model						Component	Reference
1	***Elastic plastic***							
	ρ	E		ν			femur and patella (cortical bone)	Keller et al. 1990 Currey et al. 1997 Brown et al. 1984 Lotz. et al. 1991 Choi et al. 1990
	2,000	2 (femoral head) 6 (femoral neck & condyle) 13.5 (shaft)		0.3				
2	***Elastic plastic***						tibia and fibula (cortical bone)	Burstein et al. 1976
	ρ	E	ν					
	2,000	17.5	0.3					
3	***Elastic plastic***							
	ρ	E		ν	σ_Y		femur, tibia, fibula and patella (trabecular bone)	Martens et al. 1983 Linde et al. 1989
	1,100	0.7 (femoral head) 0.4 (femoral neck & condyle) 0.2 (intertrochanter) 0.445 (tibia & fibula)		0.3	5.3			
4	***Elastic plastic***						medial and lateral menisci	Haut Donahue et al. 2003
	ρ	E	ν	σ_Y				
	1,100	6.16	0.3	66				
5	***Piecewise linear plasticity***						femur and tibia tendon	Johnson et al. 1996
	ρ	E	ν	σ_Y				
	1,000	1.2	0.3	S.S.C.				
6	***Elastic***						articular cartilage (femur, patella and medial and lateral tibia)	Froimson et al. 1997
	ρ	E	ν					
	2,000	0.2	0.2					
7	***Elastic***						skin	Puso and Weiss 1998 Mattei et al. 2008
	ρ	E	ν					
	1,000	0.001	0.45					
8	***Soft tissue visco elastic***						ACL, PCL, MCL, LCL	Puso and Weiss 1998 Untaroiu et al. 2005
	ρ	C1	C2	C3	C4	C5		
	1,000	6.8	0	0.42	58.9	279.3		
	Simplified rubber/foam						flesh	Untaroiu et al. 2005 Yamada 1970
	ρ	k	mu	g				
	1,050	2,000	0.4	0.04				

ν – Poisson ratio, σ_Y – yield stress (MPa), ρ – density (kg/m^3), E – elastic modulus (GPa),
k – bulk modulus (MPa), mu – damping coefficient, g – shear modulus (MPa), S.S.C. – stress-strain curve

Proximal femur quasi-static compression

The proximal femur is a frequently injured region in the vehicle frontal crashes, so its injury response is important for the biofidelity of the occupant LX FE model. The fracture data recorded in the compression quasi-static tests (Keyak et al. 1998) was used to validate the femoral head and neck response in two loading configurations. In the stance configuration, the femur was positioned at a 20º angle from the femur longitudinal axis to the vertical axis in the coronal plane (Fig. 5a) and the femoral shaft model was fully constrained. A molded impactor, with the material properties of polymethylmethacrylate (PMMA) and diameter of 30 mm, vertically compressed the femoral head at a compression rate of 0.5 mm/s. In the fall configuration, the proximal femur was positioned with its shaft longitudinal axis at 60 º to the vertical axis and at 70 º to the major axis of the elliptical cross-section of the femoral neck (Fig. 5b). The great trochanter was placed onto moldable PMMA material type bedding and the femoral shaft was fully constrained. A molded PMMA impactor, with a diameter of 30 mm, vertically compressed the femoral head at a rate of 0.5 mm/s until fracture. The impactor was horizontally unconstrained to minimize the transverse force. The first peak of the force recorded between the impactor and the femoral head was assumed as the femur fractures (Keyak et al. 1998) and are used for femoral head response validation. The implicit solver of DYNA 971 was used to simulate these quasi-static tests.

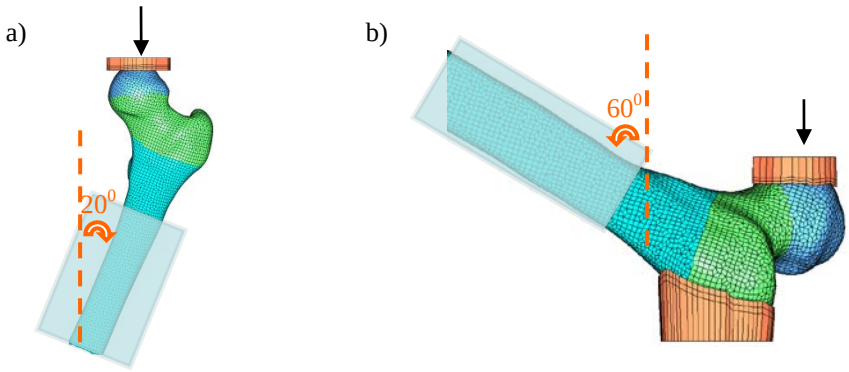

Figure 5 Femoral head quasi-static compression FE model setup of a) stance and b) fall configuration. (Untaroiu et al. 2012)

Leg combined loading

The distal third section of tibia has the highest risk of fracture during frontal crashes (Ivarsson et al. 2008). The fracture mechanism of the tibia shaft is usually assumed to be caused by the normal and bending stresses due to the intruding footwell and inward deforming dashboard, respectively (Taylor et al. 1997). Therefore, a series of PMHS tests were performed to investigate the leg injury tolerance in combined axial compression and bending loading (Untaroiu et al. 2008). The recorded test data were used in this study to validate the injury response of the leg model. The longitudinal axes of the tibia and fibula shafts were kept horizontal, with their epiphyses embedded in the PMMA cups. A ramp-increased axial compression force was applied first along the longitudinal axis of the tibia up to 20 ms. Then, an impactor with a displacement rate of 1.5 m/s loaded the leg at the center of the distal third section of the tibia along the anterior-posterior (A-P) direction of the leg (Fig. 6). Five tests with a pre-loaded axial compression force of 2, 4, 6, 7, and 8 kN were simulated. At the instant of tibia fracture, the applied bending moments ($M_{applied}$) generated by the impact force (F_i) at the center tibial distal third section were calculated for all five cases and then compared to the test results (Untaroiu et al. 2008).

$$M_{applied} = F_i d_{mj} (1 - d_i / d_j) \quad (2)$$

Where d_{mj} and d_i represent the distance from the middle of distal third part to the distal universal joint and the impactor location, respectively. The distance between the universal joints is d_j.

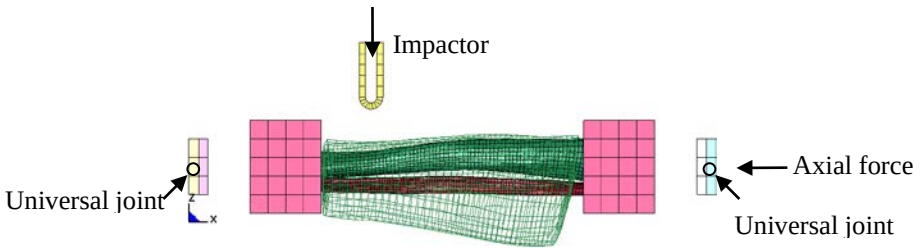

Figure 6. Leg combined loading FE model setup (Untaroiu et al. 2012).

Knee ligament (PCL) stretching

The dynamic knee stretch test conducted by Balasubramanian in 2004 was used for the validation of PCL ligament response. All soft tissues (except the PCL), the patella and the fibula were removed from the knee model. The femoral shaft was constrained and a cross-section plane was defined across the femoral shaft to record the reaction force. The knee was positioned at a flexion angle of 90^0 (Fig. 7), and a constant velocity of 1.8 m/s was imposed to the tibia shaft along the A-P direction. The time history of the reaction force data was processed using a 600 Hz SAE low-pass filter, as in Balasubramanian's tests.

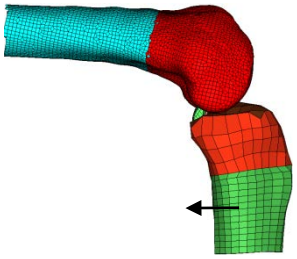

Figure 7 Knee ligament (PCL) stretch loading FE model setup (Yue et al. 2012).

The longitudinal length and middle cross sectional area of the PCL model were compared with the averaged human PCL values (Table 2). It was found that both the length and area of the PCL model were slightly smaller than the reported average PCL (Takahashi et al. 2000). Therefore, the simulated force-displacement curve was scaled to that of the averaged human level. The length scale factor λ_L and the cross section scale factor λ_c were defined as the ratio of the PCL model data to that of the averaged human data (Untaroiu et al. 2005) and a similar scaling approach as that used to the femoral shaft three-point test data was applied.

Table 2. The geometrical characteristics of PCL (Yue et al. 2012).

PCL geometrical characteristics	**PCL model**	**Averaged human PCL** (Takahashi et al. 2000)
Length (mm)	37	41
Cross sectional area (mm^2)	60	77

Knee-thigh (KT) impact

The biomechanical and injury response of KT during a typical frontal impact loading impact was validated using the test data reported by Rupp et al. in 2004. During testing the knee flexion angle was 90 º and a simulation was conducted to obtain the model geometry in this position from initial position with knee flexion angle of 120º (Fig. 8a). Minor adjustments were conducted to re-position the patella according to the pre-test CT image of the patella (Fig. 8b). Then, the femoral head was transnationally constrained using a fixed cup, and a molded rigid impactor impacted the knee region along the longitudinal axis of the femur until the bone fracture (Fig. 9a). The average displacement time history recorded in testing was imposed to the FE impactor model and the impact force time history calculated during the simulation was compared with

corresponding data measured behind the mold rigid impactor. As in testing, the force data was processed using a 300 Hz ButterWorth low-pass filter.

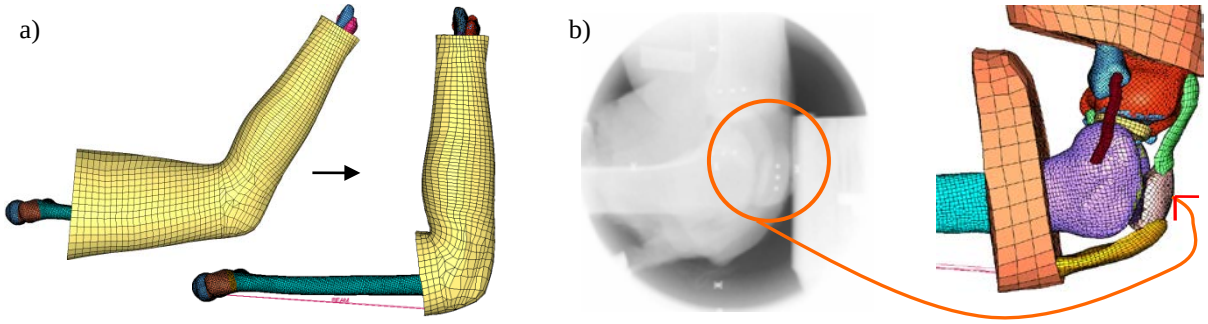

Figure 8 a) Knee flexion angle change from 120^0 to 90^0 (Yue et al. 2012) b) Verification of FE patella position to the pre-test CT image of the sample (Rupp et al. 2004).

Knee-thigh-hip (KTH) impact

The lower limb model (Untaroiu et al. 2012) and the pelvis FE model (Kim et al. 2012) were assembled together by connecting the femoral head to the acetabulum using the femoral head ligament and the hip joint capsule (Fig. 9b) modeled by beam and shell elements (thickness of 3.3 mm based on Stewart et al. 2002), respectively. To further validate the LEX model, the KTH test conducted by Rupp et al. in 2004 was simulated. As in the test configuration, the femoral mid-distal to the head axis was perpendicular to the pelvis coronal plane, and the thigh-to-pelvis angle was positioned in a standard automotive-seated posture which refers to 120^0 between the long axis of the femur and the plane defined by the anterior-superior iliac spines and the pubic symphysis (Schneider et al. 1983). The pelvis model was rigidly fixed by fully constraining the iliac wings. A molded rigid impactor impacted the knee surface along the axis defined by the mid-distal femur and femoral head with the average displacement time history recorded in testing, which is representative of the knee-to-knee bolster frontal crash rate. The impact force time history was filtered using 300 Hz ButterWorth low-pass filter as in testing, and compared with corresponding test data for the model validation.

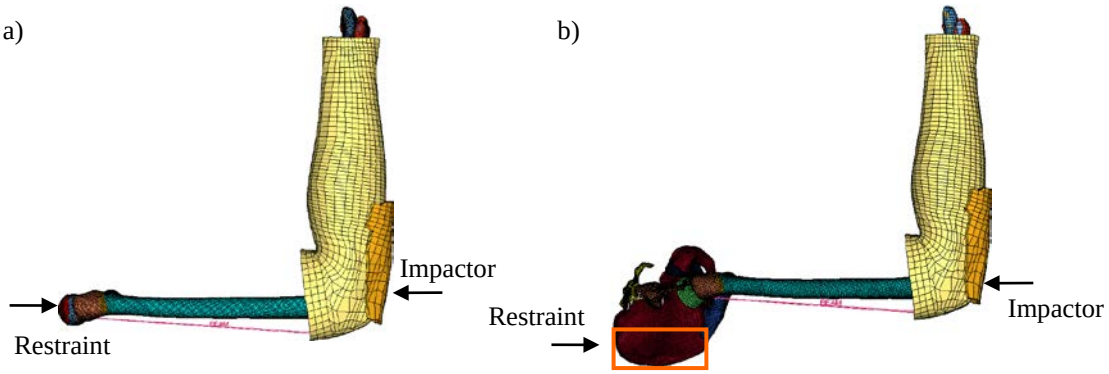

Figure 9 a) Knee-thigh and b) knee-thigh-hip impact FE models setup (Yue et al. 2012).

3. Application of the thigh-knee-leg FE model

The validated KTH model was then used to investigate the sensitivity of pelvis injury tolerance with respect to the hip joint angle. This study required two steps: first the KTH tests conducted by Rupp et al. (2003) was replicated by simulation with -30^0 hip joint angle in flexion and -10^0 in abduction; then a sensitivity study with various hip joint angle cases (flexion + abduction) was performed to investigate the correlation between the hip joint angle and the acetabulum fracture force (Fig. 10). The injury mechanism was investigated based on the peak values of von Mises stress distributions on acetabulum for different angle combinations. The hip joint rotation center was defined as the geometrical center of the femoral head ball (Veeger 2000). Compared to Rupp et al.'s tests in terms of abduction angle, in the sensitivity study the pelvic transverse axis was always perpendicular to the impact direction and the femoral shaft was rotated relative to

the pelvis to get various hip joint abduction angles. This approach tried to replicate the occupant loading throughout the KTH complex in a configuration similar to that observed in the real-world frontal impacts.

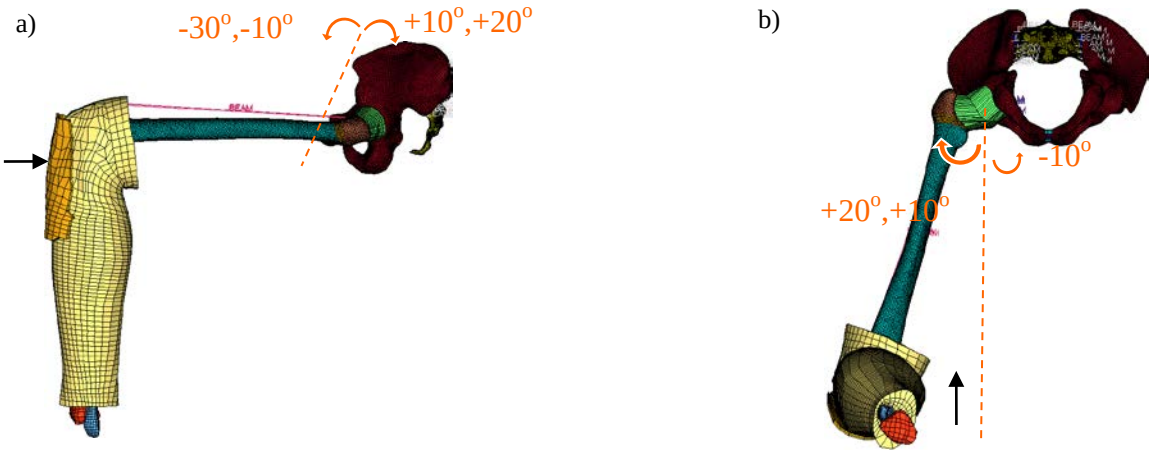

Figure 10 The schematics of the hip joint a) flexion rotation and b) adduction rotation. The arrow indicates the impact direction (Yue et al. 2012).

RESULTS

1. Development of the thigh-knee-leg FE model.

The whole thigh-knee-leg FE model of both sides (left and right) has 167,625 deformable elements (139,579 solid and 28,046 shell) and 176,978 nodes (Fig. 11a). The majority of the solid elements are hexahedral (98%), and the rest of them are pentahedral (1.9%) and tetrahedral (0.1%). While the element sizes of flesh and skin elements are in a range from 6 to 15 mm, the mesh of other parts is much more refined (element sizes in a range of 1.5 to 3 mm). The cortical shell thickness calculated by the customized MATLAB code was verified by comparing its nodal thickness to the corresponding cortical bone thickness measured manually in HyperMesh 10.0. The model has a good quality mesh (e.g. the jacobian of solid and shell elements is above 0.3 and 0.4, respectively) and the time step for explicit solver is 0.3 μs (with 0.35% mass added by mass scaling). The masses of the thigh and leg models, assigned with the appropriate densities reported in Table 1, are calculated and compared with the corresponding masses reported by Chandler et al. in 1975 based on six 50th percentile male PMHS (Table 3). The thigh and leg masses fall within one standard deviations of the corresponding reported masses.

Table 3. Lower limb mass comparison.

Source	Thigh Mass (kg)	Leg Mass (kg)
Chandler et al. 1975	6.523 ± 1.768	2.685 ± 0.553
FE model	6.494	2.897

2. Validation of the thigh-knee-leg FE model.

Femoral shaft three-point bending

During the simulation the femoral shaft fracture occurred beneath the impact location, as in experiments, at about 3.8 kN impact force which was within the range of the experimental data (3 to 5.1 kN). The force-deflection response predicted by the femur model was compared with five scaled PMHS (age 64 ± 6 years). The global response of the model was mostly linear and close to the corresponding test data (Fig. 11b). In conclusion, the simulation results showed that the femur FE model subjected to mid-shaft dynamic

bending could replicate the global biomechanical response (force-deflection curve) as well as the injury response.

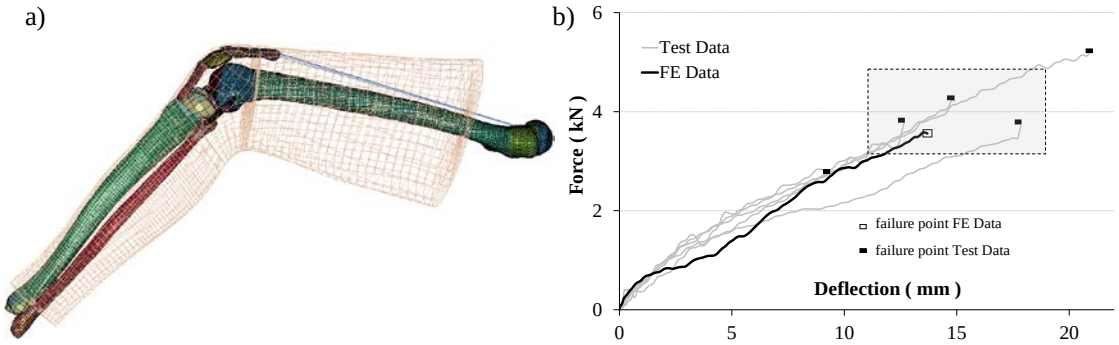

Figure 11. a) Occupant left LEX FE model lateral overview. b) The response of femoral shaft under three-point bending loading (Untaroiu et al. 2012)

Femoral shaft combined loading

For all the loading conditions of this validation scenario, femur FE model predicted shaft fractures close to the impact locations, as it was observed in testing. The impact bending moments at the time of fracture decreased from 394 Nm (pure bending case) to 75 Nm (16 kN axial compression force case) for the P-A impact cases (Fig. 12). This behavior could be explained by the induced bending moment (proportional to the pre-loaded axial compression force) which generated the bone fracture at lower levels of the impactor load than in pure bending. However in A-P impact cases, the induced moment produced by the axial compression force was compensated in the initial impact period by the applied bending moment due to the initial anterior bowing of the femoral shaft. The effect of the induced moment was much lower and the bone fracture was mostly caused by the applied moment for the A-P cases. Since the total bending moment for femoral shaft fracture is almost constant, the applied bending moments caused by the impact force at failure should to be quasi-constant for the A-P cases, as shown in the test data and the simulation result (Fig. 12). Generally, the predicted applied bending moments fall within the range, whereas towards the lower bound, of the test data.

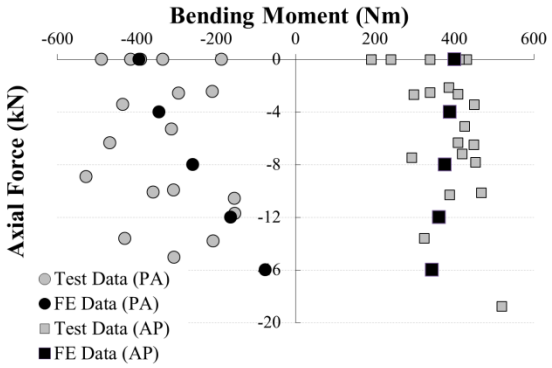

Figure 12. The femoral injury tolerance under combined axial force and mid-shaft impact force: FE simulation vs. Test Data (Untaroiu et al. 2012).

Proximal femur quasi-static compression

The fractures in the FE simulations of the stance and fall configurations occurred at the femoral neck base and intertrochanteric region (Fig. 13a), which generated a force drop in the compression force at 7.5 kN and 3.29 kN, respectively. In the testing, about 95% (17 out of 18 cases) of all fractures in stance configuration were observed in the subcapital region and 50% of all fractures in fall configuration were observed in the intertrochanteric region (Keyak et al. 2001). The mean fracture forces, as well as the standard deviations (SD), of the stance and fall configurations were 8.4 ± 3 kN and 2.38 ± 1.31 kN, respectively. The

results suggest that the proximal femur FE model can accurately predict both the fracture locations and the forces in both loading configurations.

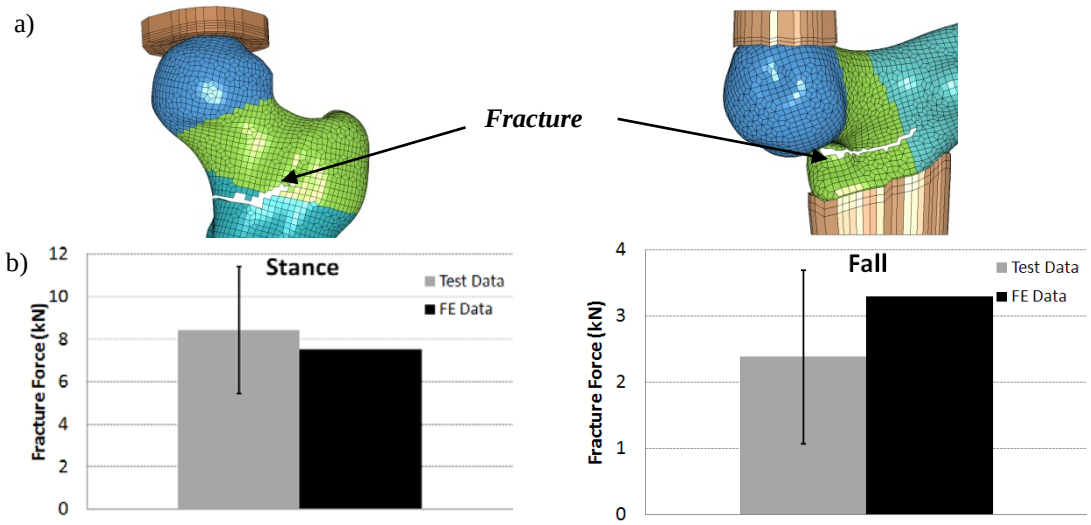

Figure 13. a) The fracture locations and b) the fracture force comparisons of the proximal femur compression tests in both stance and fall configurations (Untaroiu et al. 2012).

Leg combined loading

In the FE simulations of all five loading conditions, fractures occurred at the distal third section of tibia, and then after about 2 ms at the distal end of fibula. The impactor force at the time of the fracture decreased from 2.12 kN (2 kN axial compression force case) to 1.5 kN (8 kN axial compression force case). The predicted applied bending moments were calculated based on the Eq. 2 and the impact forces at bone fracture showed the similar decreasing trend as the test data (Fig. 14), while falling on the upper edge of the test data range.

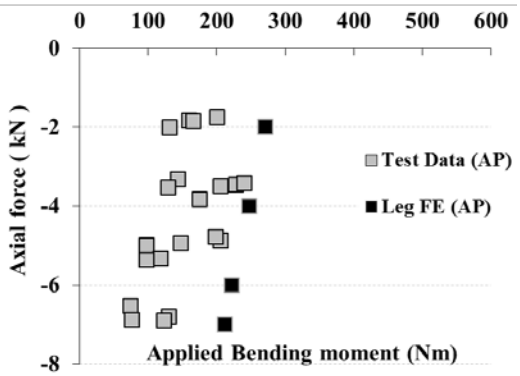

Figure 14. a) Applied bending moment comparison at instant of fracture (Untaroiu et al 2012).

Knee-ligament (PCL) stretching

The scaled simulated force-displacement response of the knee ligament model (PCL) was plotted together with the test data (Fig. 15). As it can be observed, the model stiffness and failure strength were within the ranges of test data.

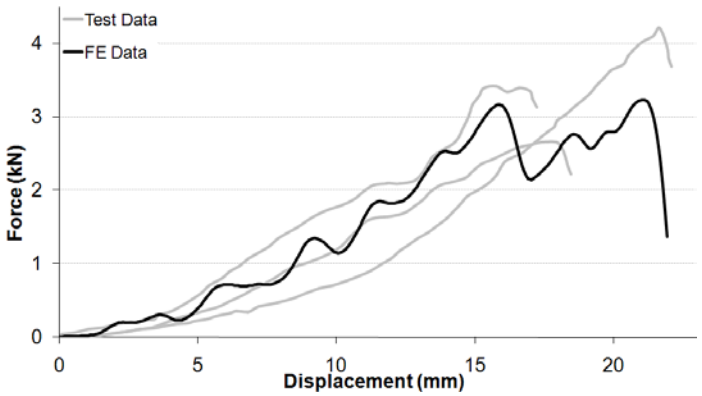

Figure 15. Force-displacement response comparison of the PCL stretch test: FE data vs. test (Yue et al. 2012).

Knee-thigh (KT) impact

In KT impact simulation, a femoral neck fracture, a frequent fracture pattern observed in testing, was recorded at around 13 ms after impact (Fig. 16a). The time history of impact force recorded in FE simulation was close to the upper bound of the test data, with a fracture force of 6.9 kN (Fig. 16b). The FE results indicated that the thigh-knee-leg model predicts accurately both the injury patterns and global kinematics of the lower limb under knee impact loading.

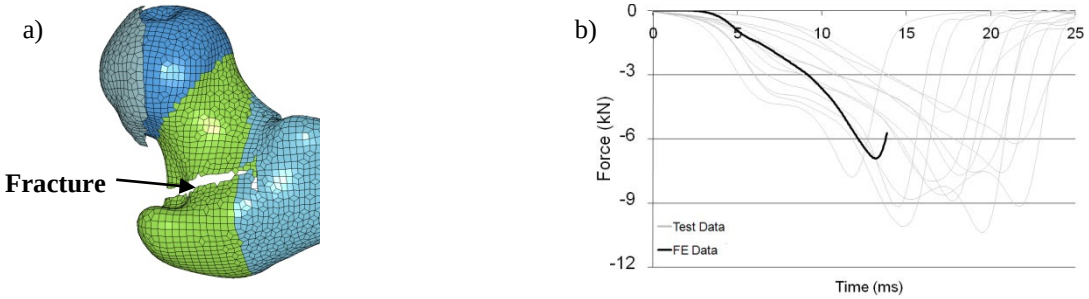

Figure 16. KT impact simulation results of a) fracture location and b) impact force time history comparison (Yue et al. 2012).

Knee-thigh-hip (KTH) impact

A pelvic acetabulum fracture pattern was predicted by the FE simulation of the KTH impact test (Fig. 17a), as it was reported in testing. In addition, the time history of the impact force calculated in FE simulation showed to be close to the upper bound of the test data, with the acetabulum fracture recorded around 5.5 kN (Fig. 17b). In conclusion, the model response was within the test data range and the fracture force, location, and time matched reasonably the test data.

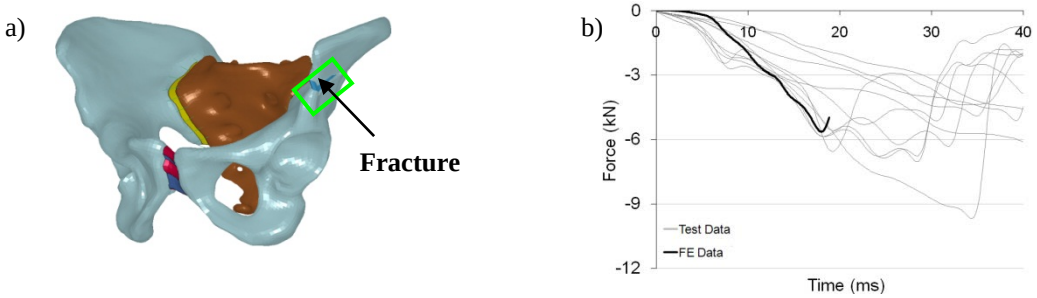

Figure 17. KTH impact simulation results of a) fracture location and b) impact force time history comparison (Yue et al. 2012).

3. Application of the thigh-knee-leg FE model

In the first part of replicating previous KTH tests (Rupp et al. 2003), the model showed a 12% decreased acetabulum fracture force in -30 ^{0} flexion posture (relative to the fracture force in neutral posture), and 4.2% decreased acetabulum fracture force in -10 ^{0} abduction posture.

In the second part of the sensitivity study, 20 KTH simulations with combined flexion (-30^0, -10^0, 0^0, 10^0, 20^0) and abduction (-10^0, 0^0, 10^0, 20^0) hip joint angles were conducted and the hip fracture forces, as well as the corresponding fracture locations, were recorded (Table 4). It was found that the hip acetabulum was more vulnerable to the frontal impacts than the proximal femur. It was observed that a third-order polynomial equation provided a good fit (R^2=0.918) to the hip fracture force data (Table 4). According to the injury tolerance surface obtained (Fig. 18), the tolerance of the hip acetabulum cortical bone was more sensitive to the hip flexion angle, rather than to the abduction angle. For an increase of hip flexion angle from -30 ^{0} to 20 ^{0}, it was observed an increase of hip acetabulum tolerance of 16% ~ 36%.

Table 4. Sensitivity study matrix of the hip joint angle for the injury tolerance (Yue et al. 2012).

		Abduction (^{0})			
		-10	0	10	20
Flexion (^{0})	20	6.27 kN (F.F.) Acetabulum (F.L.)	7.44 kN acetabulum, femoral neck	6.65 kN femoral neck, acetabulum	6.67 kN femoral neck
	10	6.01 kN acetabulum	6.69 kN acetabulum	6.42 kN acetabulum, small femoral neck	6.53 kN acetabulum, small femoral neck
	0	5.93 kN acetabulum	6.19 kN acetabulum	6.39 kN acetabulum, small femoral neck	6.42 kN acetabulum, small femoral neck
	-10	5.52 kN acetabulum	6.02 kN acetabulum	6.11 kN acetabulum	5.88 kN acetabulum, small femoral neck
	-30	5.37 kN acetabulum	5.45 kN acetabulum	5.55 kN acetabulum	5.58 kN acetabulum

F.F.: fracture force; F.L.: fracture location.

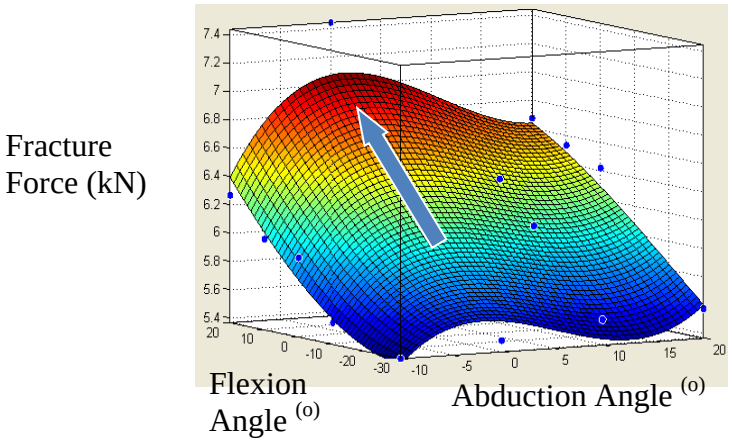

Figure 18. The injury surface of hip tolerance for various occupant postures (Yue et al. 2012).

The hip abduction angle was kept as neutral posture (0^0) and the hip flexion angle was varied form -30^0 to 20^0 (Fig. 19). The von Misses stress contours of the hip acetabulum cortical bone recorded in the

corresponding simulations showed a tendency of stress concentration in iliac wing as the flexion angle decreases. This change implied a decrease of the hip injury tolerance and caused a hip fracture at an earlier and lower impact force stage.

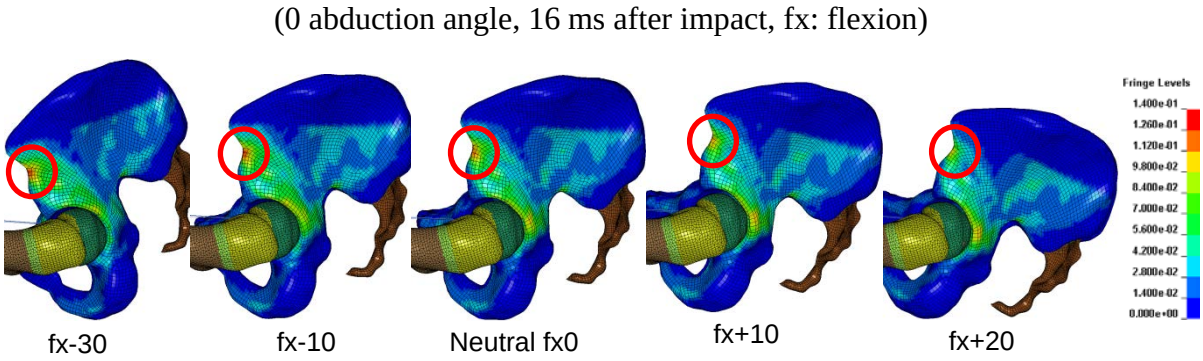

Figure 19. Von Mises stress comparison (in GPa) of acetabulum cortical bone in various hip joint flexion angles. Red circles emphasize the concentrated stresses (Yue et al. 2012).

DISCUSSION

Since the model geometry was achieved directly and only from the medical images of a 50th percentile male, it avoids the inherent geometry inaccuracy through scaling. Both the structural and unstructural mesh approaches were utilized for the appropriate corresponding components to achieve a detailed and good quality mesh. The cortical layers of the long bone shaft areas, the knee ligaments and tendons were all represented by 3D hexahedral elements, instead of 1D (bar) and 2D (shell) elements implemented by most of the previous models. The masses of the model components matched well with the literature data, which indicates the current LEX FE model approximates well the inertial properties of a 50th percentile male LEX. The time step and the associated increased mass were finely adjusted to a reasonable range to enhance the model usability for crash simulations, given the current computational power.

For the first part of the model application study, the KTH model had a similar trend of decreasing the hip injury tolerance if the flexion or the abduction angle of the hip joint decreases, as reported by Rupp et al. in 2003. From the second part of the application study of the hip joint effect for the acetabulum injury tolerance, the results suggested that a sitting posture with a larger hip joint flexion angle would increase the hip injury tolerance during frontal impacts.

For the test data of the femoral head compression validation, the fracture location reported from tests was primarily based on visual detection and the fracture force was defined as the first peak force of the compression force time history curves (Keyak et al. 1998, 2001). Since the fracture location was identified after the test, it was impossible to check the coincidence of the first peak compression force with the incidence of the bone fracture. Besides, no compression force time history curve was reported for both of the stance and fall configurations, which makes it impossible to establish a corridor to validate the femoral head response during the whole compression period. Any improvements of the test data with regards to the above points would better tune the model response.

The biomechanics of the patella is important for assessing frontal crash injuries with respect to the occupant LEX; however, to the best of our knowledge, the material properties of patellar cortical bone are still under development in the literature. Thus, the material properties of the femoral cortical bone are preliminarily assigned to the cortical shell elements of the patella.

Since the relationships of the CT Hounsfield value, the bone ash density, and the corresponding elastic modulus are starting to be established in the literature (Duchemin et al. 2008), in the future, a feasible way of assigning more accurate material properties of trabecular and cortical bone would be to use Hounsfield values of volunteers' CT scans to improve the lower limb model. In addition, a material model with asymmetric material properties in tension and compression is necessary to be developed in LS-Dyna in order to more accurately simulate the mechanical properties of cortical bone.

There is no active muscle modeled in the current study, mainly due to the lack of accurate material properties and test data for active muscle validation. However, active muscle in the thigh region is important for the occupant biomechanical responses during frontal impacts. It could provide some extra load during the automotive crashes due to muscle excitement and thus decrease the global load threshold for injury causation. Therefore, including the active muscle effect could reflect more realistic occupant injury responses.

The geometries of some parts, such as hip joint capsule and femoral head ligaments, are approximated based on literature and anatomy books due to the lack of the corresponding geometrical data and their biomechanical importance for the model responses. A better representation of these geometries, such as accurate modeling of the hip joint capsule thickness distribution, would improve the rotational biofidelity in the hip region of the model.

There is a variance of the mesh density between the distal femur and the tibia plateau, which is mainly caused by different meshing approaches. Even though the model is comprehensively validated including the knee region, a matchable mesh density between two neighboring parts would increase the model contact stability for simulation and stress/strain comparability for post-analysis. Therefore, the mesh density in the tibia plateau has a potential to be further improved to be identical with distal femur.

More validation cases, such as the thigh side impact, are necessary in the future to investigate the model lateral impact response. However, this validation case is not included in current study due to the lack of proper test data and flesh material properties.

The thigh-knee-leg FE model developed in this study is the first step towards developing a detailed and biofidelic full-body occupant FE model for CII research. After all other body region FE models are developed and integrated, this model has the potential to accurately study the injury mechanisms and predict the injury levels for occupants during frontal impacts.

CONCLUSIONS

A detailed and biofidelic occupant thigh-knee-leg FE model was developed and comprehensively validated in this study. The model geometry was directly achieved from a 50^{th} percentile male and the model mesh was created using both the structural and unstructural mesh approaches for the good mesh quality. The strain-rate dependent material model was assigned to the bony structure (cortical) for more accurate mechanical response during dynamic loading. The model was comprehensively validated globally (force/deflection) and locally (fracture location). The model responses correlate well with the corresponding test corridors and injury data. The sensitivity study results using the validated KTH model indicate that the hip posture (i.e. the flexion and abduction of the femoral shaft relative to the pelvis) affects the injury tolerance of the acetabulum cortical bone during frontal impacts.

ACKNOWLEDGEMENTS

Funding for this study was provided by the Global Human Body Models Consortium, LLC (GHBMC) through grant: PLEXM-001.

REFERENCES

BALASUBRAMANIAN, S., BEILLAS, P., BELWADI, A. et al. (2004), “Below Knee Impact Responses using Cadaveric Specimens”, Stapp Car Crash Journal, 48: 71-88

BEILLAS, P., BEGEMAN, P. C., YANG, K. H. et al. (2001), Lower Limb: Advanced FE model and New Experimental Data, Stapp Car Crash Journal, 45: 469-494.

BROWN, T. D. and FERGUSON, A. B. (1980), Mechanical Property Distributions in the Cancellous Bone of the Human Proximal Femur, Acua Orthopaedica Scandinavica, 51: 429-437.

BROWN, T. D. and VRAHAS, M. S. (1984), “The Apparent Elastic Modulus of the Juxtarticular Subchondral Bone of the Femoral Head”, Journal of Orthopaedic Research, 2: 32-8. doi: 10.1002/jor.1100100110

BURSTEIN, A. H., REILLY, D. T. and MARTENS, M. (1976), “Aging of Bone Tissue: Mechanical Properties”, Journal of Bone Joint Surgery, 58A: 82-6.

CHANDLER, R. F., CLAUSER, C. E., MCCONVILLE, J. T. et al. (1975), “Investigation of Inertial Properties of The Human Body”, Report AD-A016 485 for NHTSA.

CHOI, K., KUHN, J. L., CIARELLI, M. J. et al. (1990), “The Elastic Moduli of Human Subchondral, Trabecular, and Cortical Bone Tissue and the Size-Dependency of Cortical Bone Modulus”, Journal of Biomechanics, 23 (11): 1103-13. doi:10.1016/0021-9290(90)90003-L

CRANDALL J.R., BOSE D., FORMAN J., ARREGUI-DALMASES C., UNTAROIU C.D., SHAW C.G., KERRIGAN J.R. (2011) A Review of Human Surrogates for Injury Biomechanics Research, Clinical Anatomy, 24(3): 362-371.

CURREY, J. D., FOREMAN and LAKETIC, J. (1997), “Effects of Ionizing Radiation on the Mechanical Properties of Human Bone”, Journal of Orthopedic Research, 15. doi: 10.1002/jor.1100150116

DUCHEMIN, L., BOUSSON, V., RAOSSANALY, C. et al. (Apr. 2008), Prediction of Mechanical Properties of Cortical Bone by Quantitative Computed Tomography, Medical Engineering Physics, 30(3):321-8. doi: 10.1016/j.medengphy.2007.04.008

EVANS, F.G., KING, A.I. (1961), “Regional Differences in Some Physical Properties of Human Spongy Bone”, Biomechanical Studies of the Musculoskeletal System, Springfield.

HAUT DONAHUE, T. L., HULL, M. L., RASHID, M. M. et al. (2003), “How the Stiffness of Meniscal Attachments and Meniscal material Properties Affect Tibio-Femoral Contact Pressure Computed using A Validated Finite Element Model of the Human Knee Joint”, Journal of Biomechanics, 36: 19-34. doi: 10.1016/S0021-9290(02)00305-6

FOSTER, J. K., KORTGE, J. O. and WOLANIN, M. J. (1977), “Hybrid III – A Biomechanically-Based Crash Test Dummy”, SAE 770938. doi: 10.4271/770938

FROIMSON, M. I., RATCLIFFE, A., GARDNER, T. R. et al. (1997), “Differences in Patellofemoral Joint Cartilage Material Properties and Their Significance to the Etiology of Cartilage Surface Fibrillation”, Osteoarthritis and Cartilage, 5: 377-86. doi: 10.1016/S1063-4584(97)80042-8

FUNK, J. R., KERRIGAN, J. R. and CRANDALL, J. R. (2004), “Dynamic Bending Tolerance and Elastic-Plastic Material Properties of the Human Femur”, 48th annual proceedings of AAAM.

GAYZIK, F., MORENO, D., GREER, C., WUERTZER, S., MARTIN, R., STITZEL, J. (2011) Development of a Full Body CAD Dataset for Computational Modeling: A Multi-modality Approach, Annals of Biomedical Engineering, 39(10), pp. 2568-2583.

GORDON, C. C., CHURCHILL, T., CLAUSER, C. E. et al. (1988), 1988 Anthropometric Survey of U.S. Army Personnel: Methods and Summary Statistics, Final Report (NATICK/TR-89/027) U.S. Army Natick Research Development and Engineering Center, Natick, MA.

HAUG, E. (2001), “H-Model Overview Description”, Proceedings of the Twenty-Ninth International Workshop on Human Subjects for Injury Biomechanics Research.

HEWITT, J., GUILAK, F., GLISSON, R. et al. (2001), “Regional Material Properties of the Human Hip Joint Capsule Ligaments”, Journal of Orthopaedic Research, 19 (359-64).

IRWIN, A., MERTZ, H., ELHAGEDIAB, A. et al. (2002), “Guidelines for Assessing the Biofidelity of Side Impact Dummies of Various Sizes and Ages”, 46th Stapp Car Crash Conferences, SAE 2002-22-0016.

IVARSSON, B. J., MANASWI, A., GENOVESE, D. et al. (2008), “Site, Type, and Local Mechanism of Tibial Shaft Fracture in Drivers in Frontal Crashes”, Forensic Science International, 174.

IVARSSON, B.J., GENOVESE, D., CRANDALL, J.R et al. (2009), “The Tolerance of the Femoral Shaft in Combined Axial Compression and Bending Loading”, Stapp Car Crash Journal, vol. 53, 251-290.

JOHNSON, G. A., LIVESAY, G. A., S. L-Y. WOO et al. (1996), “A Single Integral Finite Strain viscoelastic Model of Ligaments and Tendons”, Journal of Biomechanics, 118(2): 221-6. doi: 10.1115/1.2795963

KELLER, T. S., MAO, Z. and SPENGLER, D. M. (1990), "Young's Modulus, Bending Strength, and Tissue Physical Properties of Human Compact Bone", Journal of Orthopedic Research, 8. doi: 10.1001/jor.1100080416

KEMPER, A.R., MCNALLY, C., DUMA, S.M. (2008), "Dynamic Tensile Material Properties of Human Pelvic Cortical Bone", International ISA Biomedical Sciences Instrumentation Symposium.

KERRIGAN, J.R., DRINKWATER, D.C., KAM, C.Y. et al. (2004), "Tolerance of the Human Leg and Thigh in Dynamic Latero-Medial Bending", J. of Crashworthiness, 9 (6): 607-623.

KEYAK, J. H., ROSSI, S. A., JONES, K. A. et al. (1998), "Prediction of femoral fracture load using automated finite element modeling", Journal of Biomechanics, 31:125-133. doi: 10.1016/S0021-9290(97)00123-1

KEYAK, J. H., ROSSI, S. A., JONES, K. A. et al. (2001), Prediction of Fracture Location in the Proximal Femur Using Finite Element Models, Medical Engineering & Physics, 23: 657-664. doi: 10.1016/S1350-4533(01)0094-7

KIM, Y. S., CHOI, H. H., CHO, Y. N. et al. (Nov. 2005), "Numerical Investigations of Interactions between the Knee-Thigh-Hip Complex with Vehicle Interior Structures", Stapp Car Crash Journal, 49.

KIM, Y.H., KIM, J.E., EBERHARDT, A.W., "A New Cortical Thickness Mapping Method with Application to an In-Vivo Finite Element Model, Computer Methods in Biomechanics and Biomedical Engineering, (under review).

KUHN, J. L., GOLDSTEIN, S. A., CIARELLI, M. J. et al. (1989), The Limitation of Canine Trabecular Bone as A Model for Human: A Biomechanical Study, Journal of Biomechanics, 22: 95. doi: 10.1016/0021-9290(89)90032-8

KUPPA, S., WANG, J., HAFFNER, M. et al. (2001), "Lower Extremity Injuries and Associated Injury Criteria", National Highway Traffic Safety Administration, Conference on the Enhanced Safety of Vehicles, 17(457).

LESSLEY, D., CRANDALL, J. SHAW, G. et al. (2004), "A Normalization Technique for Developing Corridors from Individual Subject Responses", SAE International 2004-01-0288.

LINDE, F., HVID, I. and PONGSOIPETCH, B. (1989), "Energy Absorptive Properties of Human Trabecular Bone Specimens during Axial Compression", Journal of Orthopedic Research, 7. doi: 10.1002/jor.1100070316

LOTZ, J. C., GERHART, T. N. and HAYES, W. C. (1991), "Mechanical Properties of Metaphyseal Bone in the Proximal Femur", Journal of Biomechanics, 24 (5): 317-29. doi: 10.1016/0021-9290(91)90350-V

MAENO, T. and HASEGAWA, J. (2001), "Development of a Finite Element Model of the Total Human Model for Safety (THUMS) and Application to Car-Pedestrian Impacts", Conference on the Enhanced Safety of Vehicles, 17(494).

MARTENS, M., VAN AUDEKERCKE, R., DELPORT, P. et al. (1983), "The Mechanical Characteristics of Cancellous Bone at the Upper Femoral Region", Journal of Biomechanics, 16. doi: 10.1016/0021-9290(83)90098-2

MATTEI, C. P., BEC, S., ZAHOUANI, H. (2008), "In vivo measurements of the elastic mechanical properties of human skin by indentation tests", Medical Engineering & Physics, 30: 599-606. doi: 10.1016/j.medengphy.2007.06.011

MORGAN, R., EPPINGER, R., MARCUS, J. et al. (1990), "Human Cadaver and Hybrid III Responses to Axial Impacts of the Femur", Proceedings of the International IRCOBI on Biomechanics Impacts.

ROBBINS, D. H., SCHNEIDER, L. W. and HAFFNER, M. (1983), Seated Posture of Vehicle Occupants, Stapp Car Crash Conference Proceedings, # 831617.

RUPP, J.D., REED, M.P., EE, C.A.V. et al. (2002), "The Tolerance of the Human Hip to Dynamic Knee Loading", 46th. Stapp Car Crash Conference, 46: 211-28.

RUPP, J.D., REED, M.P., JEFFREYS, T.A. et al. (2003), “Effects of Hip Posture on the Frontal Impact Tolerance of the Human Hip Joint”, 47th. Stapp Car Crash Journal, 47: 21-33.

RUPP, J.D., REED, M.P., JEFFREYS, T.A. et al. (2004), “KTH Injury Investigations”, NHTSA report.

PUSO, M. A. and WEISS, J. A. (1998), “Finite Element Implementation of Anisotropic Quasi-Linear Viscoelasticity Using a Discrete Spectrum Approximation”, Journal of Biomechanical Engineering, 120: 62-70. doi: 10.1115/1.2834308

SCHAUER, D. A., PERFECT, S. and WEISS, J. (1997), “Finite Element Modeling of the Human Anatomic Pelvis and Leg”, National Highway Traffic Safety Administration.

SCHNEIDER, L., ROBBINS, D., PFLUG, M. et al. (1983), Development of anthropometrically based design specifications for an advanced adult anthropomorphic dummy family, In: DOT/HS 806 715, US Department of Transportation, Washington DC.

SHIN, J., YUE, N., UNTAROIU, C.D. (2012) A Finite Element Model of the Foot and Ankle for Automotive Impact Applications, Annals of Biomedical Engineering, (in press).

SILVESTRI, C. and RAY, M. H. (Apr. 2009), “Development of a Finite Element Model of the Knee-thigh-hip of a 50 percentile male including ligaments and muscles”, International Journal of Crashworthiness, 14 (2). doi: 10.1080/13588260802671399

SPETHMANN, P. and HERSTATT, C. (2009), Crash Simulation Evolution and its Impact on R&D in the Automotive Applications, International Journal of Product Development, 8 (3): 291-305. doi: 10.1504/IJPD.2009.024202

STEWART, K.J., EDMONDS, R.H., BRANDS, R.A. et al. (2002), “Spatial Distribution of Hip Capsule Structural and Material Properties”, Journal of Biomechanics 35 (1491-98).

TAKAHASHI, Y., KIKUCHI, Y., KONOSU, A. et al. (2000), “Development and Validation of the Finite Element Model for the Human Lower Limb of Pedestrians”, Stapp Car Crash Journal, 2000-01-SC22.

TAKAHASHI, Y., KIKUCHI, Y., MORI, F. et al. (2003), “Advanced FE Lower Limb Model for Pedestrians”, Conference on the Enhanced Safety of Vehicles, 18(218).

TAYLOR, A., MORRIS, A., THOMAS, P. et al. (1997), “Mechanisms of Lower Extremity Injuries to Front Seat Car Occupants-An in depth Accident Analysis”, International IRCOBI Conference on the Biomechanics of Impact, 53-72.

UNTAROIU, C., DARVISH, K., CRANDALL, J. et al. (2004), Development and Validation of a Finite Element Model of the Lower Limb, ASME International Mechanical Engineering Congress and RD&D Conference and Exposition, IMECE 2004-61583. doi: 10.1115/IMECE2004-61583

UNTAROIU, C. (May 2005), “Development and Validation of a Finite Element Model of Human Lower Limb”, Ph.D dissertation, Department of Mechanical and Aerospace Engineering, University of Virginia, Charolottesville.

UNTAROIU, C., DARVISH, K. and CRANDALL, J. (Nov. 2005), “A Finite Element Model of the Lower Limb for Simulating Pedestrian Impacts”, Stapp Car Crash Journal, 49.

UNTAROIU, C., DARVISH, K., CRANDALL, J. et al. (2005), “Characterization of the Lower Limb Soft Tissues in Pedestrian Finite Element Models”, ESV conference.

UNTAROIU, C., IVARSSON, J., GENOVESE, D. et al. (2008), “Biomechanical Injury Response of Leg Subjected to Combined Axial Compressive and Bending Loading”, Biomedical Sciences Instrumentation, 44: 141-6.

UNTAROIU, C., SALZAR, R., GUILLEMONT, H. et al. (2008), “The Strain Distribution and Force Transmission Path Through Pubic Rami During Lateral Pelvic Impacts”, ASME International Mechanical Engineering Congress and RD&D Congress, Boston.

UNTAROIU, C. (2010), A numerical investigation of mid-femoral injury tolerance in axial compression and bending loading, International Journal of Crashworthiness, 15(1):83-92. doi: 10.1080/13588260903047671

UNTAROIU, C.D. YUE, N., SHIN, J. (2012) A Finite Element Model of the Lower Limb for Simulating Automotive Impacts, Annals of Biomedical Engineering, (under review).

U.S. Department of Transportation, National Highway Traffic Safety Administration (NHTSA), "Federal Motor Vehicle Safety Standards and Regulations", http://www.nhtsa.gov/cars/rules/import/FMVSS/.

VEEGER, H.E.J. (2000), "The Position of the Rotation Center of the Glenohumeral Joint", Journal of Biomechanics, 33: 1711-15.

YAMADA, H. (1970), Strength of Biological Materials, The Williams & Wilkins Company, Baltimore.

YUE, N., SHIN, J., Untaroiu, C.D. (2012) A Numerical Investigation of Biomechanical and Injury Response of Occupant Lower Extremity during Automotive Crashes, Proceeding of ICRASH 2012 Conference, Milano, Italy